Interferometric detection of acoustic waves at air-solid interface – Applications to non-destructive testing

Frédéric Jenot, Mohammadi Ouaftouh, Marc Duquennoy, Mohamed Ourak

Interferometric detection of acoustic waves at air-solid interface applications to non-destructive testing

Cite as: J. Appl. Phys. **97**, 094905 (2005); https://doi.org/10.1063/1.1886276
Submitted: 27 May 2004 • Accepted: 15 February 2005 • Published Online: 20 April 2005

F. Jenot, M. Ouaftouh, M. Duquennoy, et al.

Interferometric detection of acoustic waves at air-solid interface applications to non-destructive testing

F. Jenot,[a] M. Ouaftouh, M. Duquennoy, and M. Ourak
Institut d'Electronique et de Micro-électronique du Nord (IEMN), UMR CNRS 8520, Département Opto-Acousto-Electronique (OAE), Université de Valenciennes et du Hainaut Cambrésis, Le Mont Houy, 59313 Valenciennes Cedex 9, France

(Received 27 May 2004; accepted 15 February 2005; published online 20 April 2005)

In this paper, some properties of acoustic waves at the air-solid interface are reviewed and laser-ultrasonics is used to optically excite and detect these waves. In comparison with the leaky Rayleigh wave, a large amplitude is observed for the acoustic disturbance which is composed of Scholte and lateral waves. However, it is apparent from theoretical results, taking source terms into account, that the normal displacement of these waves cannot be large in such an interface. Another explanation for the high-intensity fluctuation measured is the optical heterodyne detection of the refractive index variation induced in the fluid. This assumption is experimentally checked by probing the acoustic field parallel to the surface of the sample. The potentialities of these waves in non-destructive testing are also investigated. It is clearly shown that the transmitted, reflected, or diffracted acoustic fields provide useful information about the position or the size of structures intercepting the propagation path. Indeed, glass plate thickness or steel block position can be easily determined using a time of flight analysis. This suggests a lot of new applications in the sizing of structures where noncontact measurements on inaccessible parts would be necessary. © *2005 American Institute of Physics*. [DOI: 10.1063/1.1886276]

I. INTRODUCTION

Around 1925, Stoneley pointed out the existence of a surface wave between two welded semi-infinite elastic solids and about 15 years later, the geophysicist Scholte in order to understand the unexplained properties of seismograms, described a particular case of the Stoneley wave when one of the solid becomes a fluid.[1–3] This wave, nowadays called Scholte wave, has its energy mainly localized in the fluid and if the viscosity of the media is neglected, the Scholte wave propagates without attenuation. Different methods allow the generation of this wave, for example, the use of an interdigital transducer or a thermoelastic source.[4,5]

In this paper, we describe an experimental analysis of the structure and some interesting potential applications in non-destructive testing of Scholte waves at an air-solid interface.

Let us consider two homogeneous isotropic half spaces in contact at $z=0$, ρ_1 is the density of the solid and ρ_2 the density of the fluid. V_t and V_l stand for the velocities of the shear and longitudinal waves in the solid, respectively. V_f is the velocity of the compressive bulk wave in the air and V the velocity of the interface wave. The secular equation of the velocities is given by[4]

$$4\xi^2(1-\xi^2)^{1/2}(\eta^2-\xi^2)^{1/2}-(1-2\xi^2)^2-\frac{\rho_2}{\rho_1}\left(\frac{\eta^2-\xi^2}{\alpha^2-\xi^2}\right)^{1/2}=0, \tag{1}$$

where $\xi=V_t/V$, $\eta=V_t/V_l$, and $\alpha=V_t/V_f$.

Brekhovskikh[2] demonstrated in 1960 the existence of two roots of this equation; one is real and the other is complex. The real solution corresponds to the Scholte wave propagating along the interface, and its velocity is close to the lowest bulk velocity of the two media.[3]

Equation (1) is solved for the air-aluminum interface by searching a real root. The density of the solid is $\rho_1=2700\ \mathrm{kg/m^3}$ and the density of the air at a temperature of 25 °C is $\rho_2=1.16\ \mathrm{kg/m^3}$. The longitudinal and transverse wave velocities for aluminum are $V_l=5919\ \mathrm{m/s}$ and $V_t=2981\ \mathrm{m/s}$, respectively. The sound speed V_f for dry air treated as a real gas is 346.3 m/s.[6] By writing $V_s=(1-\varepsilon)V_f$, the solution of the secular equation of the velocities is approximately given by[1]

$$\varepsilon=\frac{1}{8}\left(\frac{\rho_2}{\rho_1}\frac{V_f^2V_l^2}{V_t^2(V_l^2-V_t^2)}\right)^2=7.5\times10^{-12}. \tag{2}$$

A numerical resolution of Eq. (1) provides $\varepsilon=7.7\times10^{-12}$, which is in good agreement with the previous prediction. This result shows that the velocity V_s of the

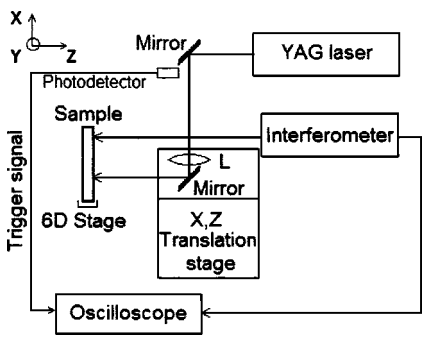

FIG. 1. Experimental setup for the laser generation and detection of the Scholte-lateral wave.

[a]Electronic mail: frederic.jenot@univ-valenciennes.fr

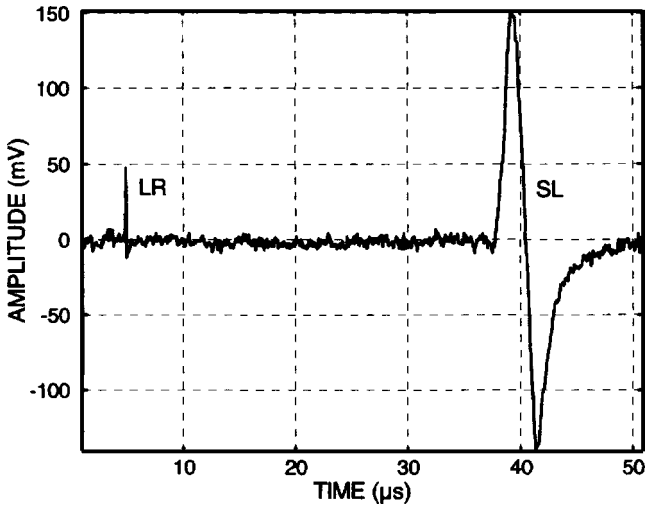

FIG. 2. Leaky Rayleigh wave (LR) in comparison with the Scholte/lateral wave (SL) for a distance of propagation $D \approx 14$ mm.

Scholte wave is very close to the velocity V_f of the longitudinal wave in the fluid. In this case, the spatial structure of the Scholte wave is similar to the structure of the quasi-one-dimensional bulk wave in the air, and the penetration depth of the Scholte wave in the fluid significantly exceeds its wavelength.[7] In the same way, the velocity of the leaky Rayleigh wave is equal to 2778.39 m/s, with a negligible imaginary part ($\simeq 10^{-4}$) which corresponds to a very weak leakage in the fluid.

It should be mentioned that a compressional lateral wave in the air associated with the branch points $\pm V_f$ in Eq. (1) is also excited and, in our case, it is impossible to separate this wave from the Scholte wave by their times of flight. In the following, we denote by SL wave the composite Scholte/lateral wave.[8] Other lateral waves associated with each bulk

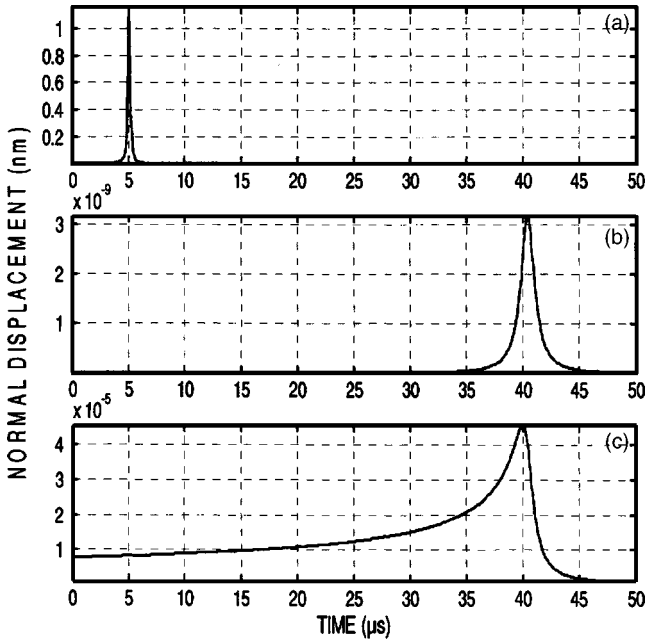

FIG. 3. Normal displacements of the leaky Rayleigh (a), Scholte (b), and lateral (c) waves computed for a propagation distance of 14 mm.

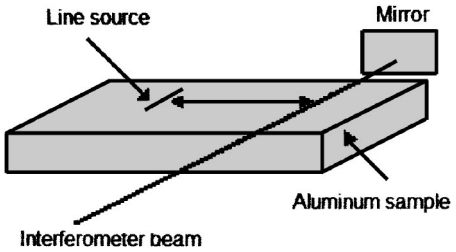

FIG. 4. Experimental configuration for the SL wave detection due to the air-index variation.

wave in the solid also exist. These waves excited by laser were often studied[9] and are not of interest in the present publication.

II. EXPERIMENTAL SETUP

The laser-ultrasonics setup is shown in Fig. 1. A 10-ns duration *Q*-switched yttrium aluminum garnet (YAG) laser pulse of 532-nm wavelength is focused with a cylindrical lens *L* on an aluminum plate as a line source of approximately 0.5-mm width and 10-mm length. The energy per pulse was 6 mJ, which allows us to work in the thermoelastic mode. The ultrasonic receiver is a Mach–Zehnder type of heterodyne interferometer with a minimum detectable displacement of about 0.1 Å. The experiments have been achieved to measure the time of flight *t* at different source-receiver distances *D* by moving the source along the *x* axis. The accuracy of the displacement of the line source is ± 0.1 μm. Figure 2 shows the leaky Rayleigh wave (LR) and the SL wave for an emitter-receiver distance of 14 mm and an averaging signal of 16 laser pulse shots. The experimental velocities of these waves deduced by the cross-correlation time delay measurement[10] for two distances of propagation are respectively 2788 m/s and 346 m/s, which are in good agreement with the theoretical velocities. The Rayleigh wave has a central frequency of 4 MHz and the SL wave, 150 kHz.

III. DISCUSSION

In order to explain the large amplitude of the Scholte wave in comparison with the amplitude of the leaky Rayleigh wave, the normal displacements of both these waves must be expressed. By the process of laser-induced thermoelastic excitation of acoustic waves, the harmonic equations of motion cannot be used. Indeed, the excitation efficiency of the different interface modes is strongly dependent on the excitation source. Consequently, we use the theory of Gusev *et al.*[8] which describes well the wave motion along a plane fluid-solid interface, taking source terms into account. The light penetration depth in aluminum is very small compared to the thermal diffusion length. Consequently, the experiment must be treated in the previous theory as the regime of a light-absorbing interface. The characteristic parameters P_R, P_S, and P_L which give the relative efficiency of the Rayleigh, Scholte, and lateral wave excitation due to air and solid heating are given by[8]

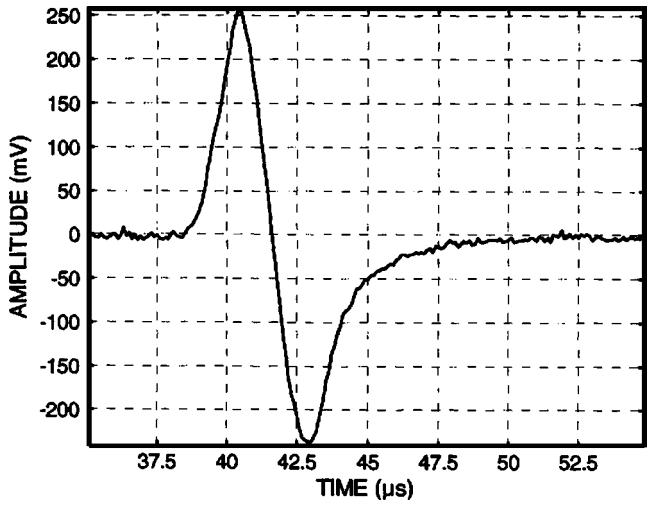

FIG. 5. Detected SL wave with the interferometer beam parallel to the surface of the sample. The distance of propagation is about 14 mm.

$$P_R = \frac{V_t^2}{2V_t^2 - V_r^2}\frac{V_l}{V_f}\frac{\sqrt{V_l^2 - V_r^2}}{\sqrt{V_r^2 - V_f^2}}\frac{\gamma_f}{\gamma_a}\frac{e_f}{e_a}$$

$$P_L \approx P_S = \frac{V_S^2}{2V_t^2 - V_S^2}\frac{V_l}{V_f}\frac{\sqrt{V_l^2 - V_S^2}}{\sqrt{V_f^2 - V_S^2}}\frac{\gamma_f}{\gamma_a}\frac{e_f}{e_a}. \quad (3)$$

Here, γ is the Grüneisen parameter and e is the thermal effusivity, where the subscripts f and a refer respectively to air and aluminum. This leads to $P_R \approx 10^{-3}$, which means that the Rayleigh wave is predominantly excited by heating the solid. Unlike this, $P_S \approx 20$ and it follows that the main contribution to the SL wave generation comes from the air. Indeed, it is possible to give relative numerical values of the energy in the substrate and air. Assuming that the wave propagates in the x direction and that the z axis is normal to the surface of the sample ($z>0$ in the air), the energy flow in the considered medium is given by the expression

$$P = \frac{-i\omega}{4}\int \left(\sigma_{zx}u_z^* + \sigma_{xx}u_x^* - \sigma_{zx}^* u_z - \sigma_{xx}^* u_x\right)dz, \quad (4)$$

where u_x, u_z are the displacements and σ_{zx}, σ_{xx} the corresponding stresses. The ratio R between the energy flow P_1 in the solid and the energy flow P_2 in the air is performed analytically in the Appendix. It is shown that $R = P_1/P_2 \approx 15.7 \times 10^{-12}$, which confirms the previous assumption and means that the wave must be very sensitive to any changes in the air properties in comparison with those of the solid. Consequently, the acoustic disturbances generated in air should cross the interface to contribute to the formation of the SL wave and to induce a normal displacement of the substrate. However, this phenomenon is strongly supressed due to the high acoustic impedance mismatch between the two media.[11]

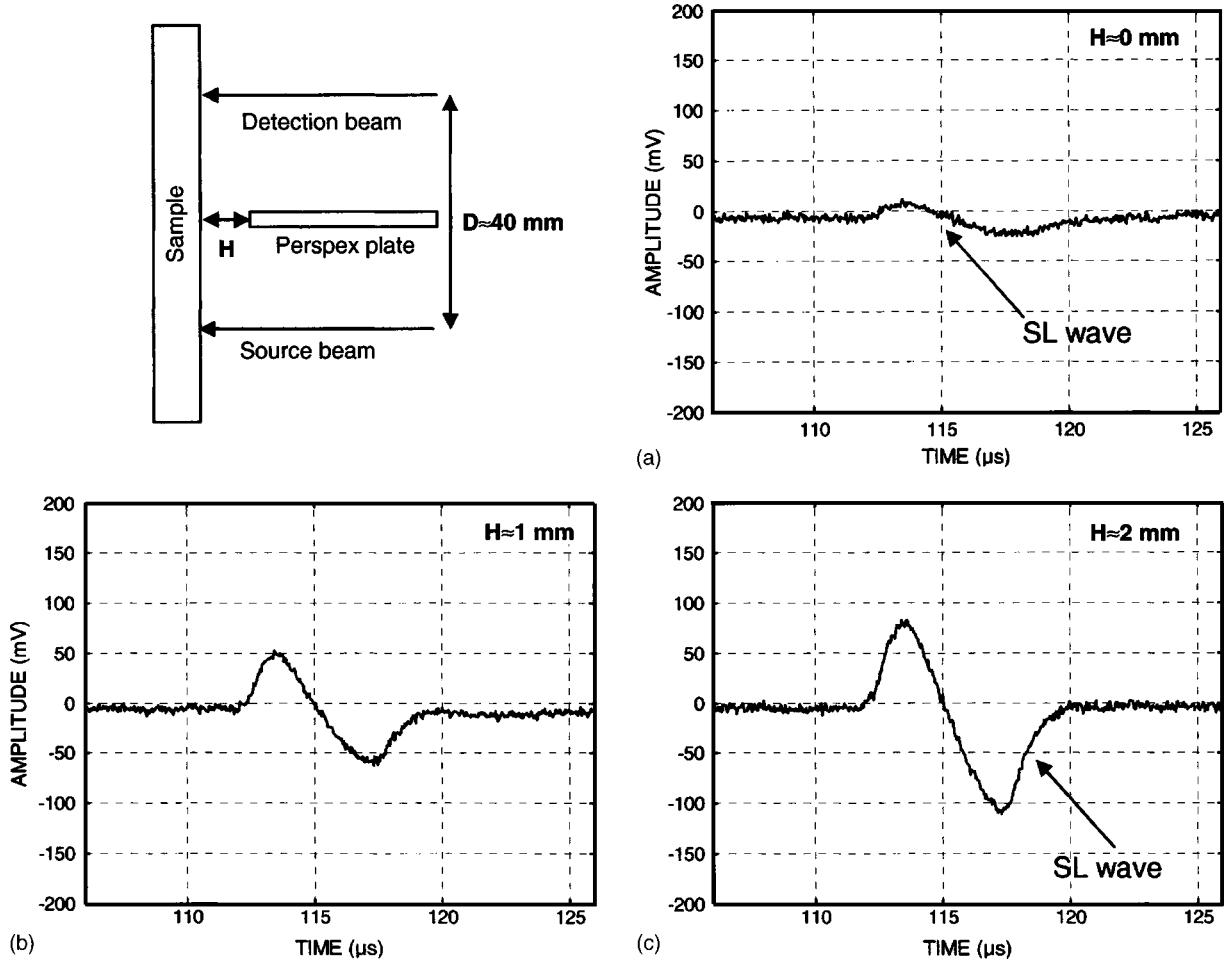

FIG. 6. Perturbation of the SL wave by a plate which comes progressively near the sample (distance H).

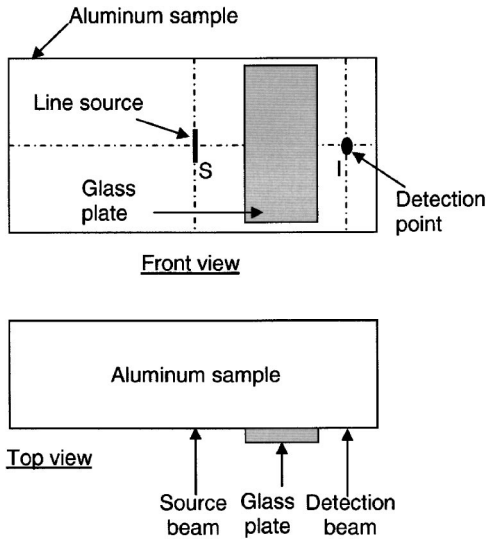

FIG. 7. Some glass plates were put down on the surface of the sample between the line source and the detection point.

In order to confirm this qualitative explanation, the normal displacements at the interface of the leaky Rayleigh, Scholte, and lateral waves are computed and presented in Fig. 3. The energy absorbed in aluminum is fixed at 1 mJ and the propagation distance is 14 mm. In this case, the results show clearly that neither the Scholte wave nor the lateral wave can be detected interferometrically by their normal displacements. The signal broadening for these waves (in comparison with the Rayleigh wave) is also well predicted by the theory.

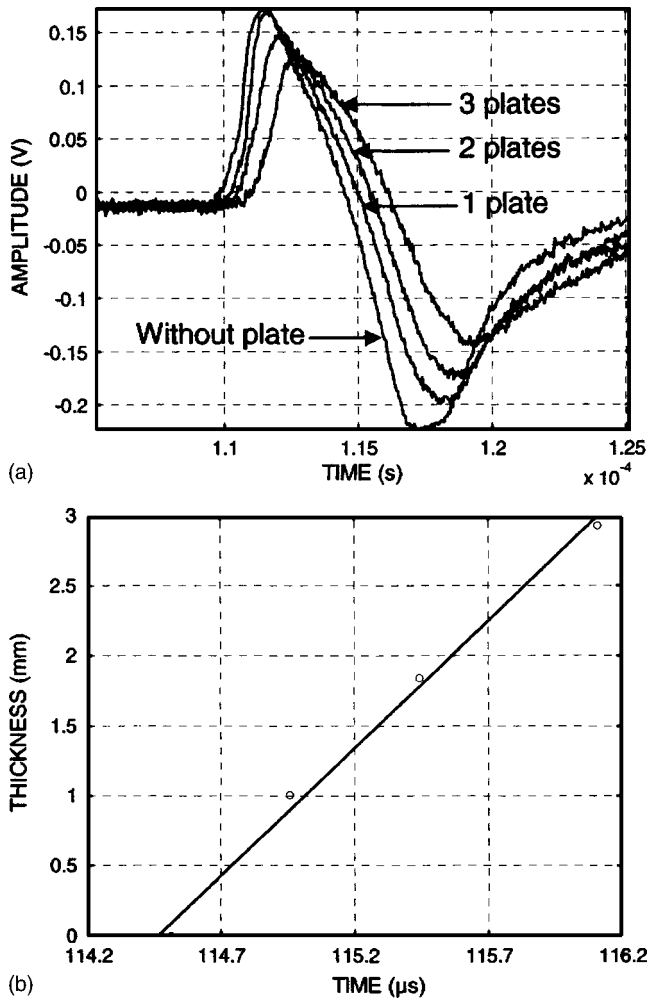

FIG. 8. (a) Time traces of the SL wave interaction with glass plates put down on the aluminum sample. (b) Plot of glass plates thickness according to the SL wave time of flight.

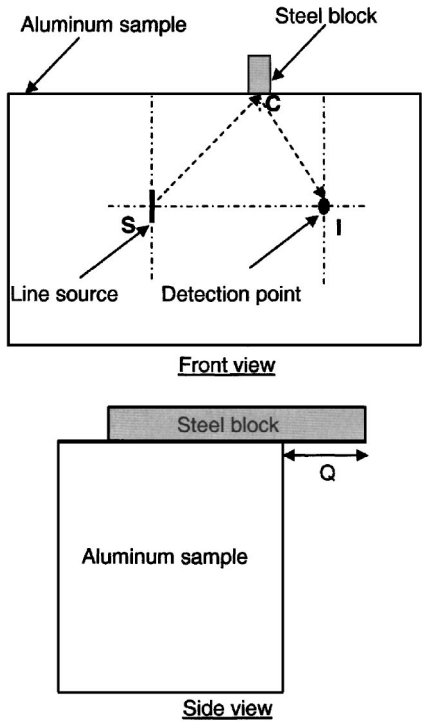

FIG. 9. A steel block comes out from the surface of the aluminum sample of a distance Q.

However, the large amplitude observed must be qualitatively discussed because the measure obtained optically is the superposition of both effects: the detection of the normal displacement and the acoustic pressure in air.[12] Precisely, the probe beam of the interferometer shifted in frequency by an acousto-optic Bragg cell (f_b=70 MHz) crosses the air where the refractive index is changed by the acoustic field. Then, the phase modulated current on the photodiode resulting from the interference of the probe beam and the reference can be written as

$$I = I_0 \cos(2\pi f_b t + \phi_1 - \phi_2 + \upsilon_i(t)), \tag{5}$$

where I_0 is the dc component of the incident light power. ϕ_1 and ϕ_2 are respectively the phase constants of the probe and reference beams of the interferometer and υ_i is the optical phase shift due to the ultrasonic wave. This one is proportional to the integrated acoustic pressure p along the path of the light across the acoustic field[13]

$$\upsilon_i(t) = \frac{4\pi\vartheta}{\lambda} \int p(z,t)dz, \tag{6}$$

where ϑ is the air piezo-optic coefficient and λ is the wavelength of the laser beam.

The bipolar shape of the SL wave is then probably due to the x derivative of the tangential motion in the fluid included in the calculus of p. The aim of our investigations is to confirm experimentally that the major contribution in the mea-

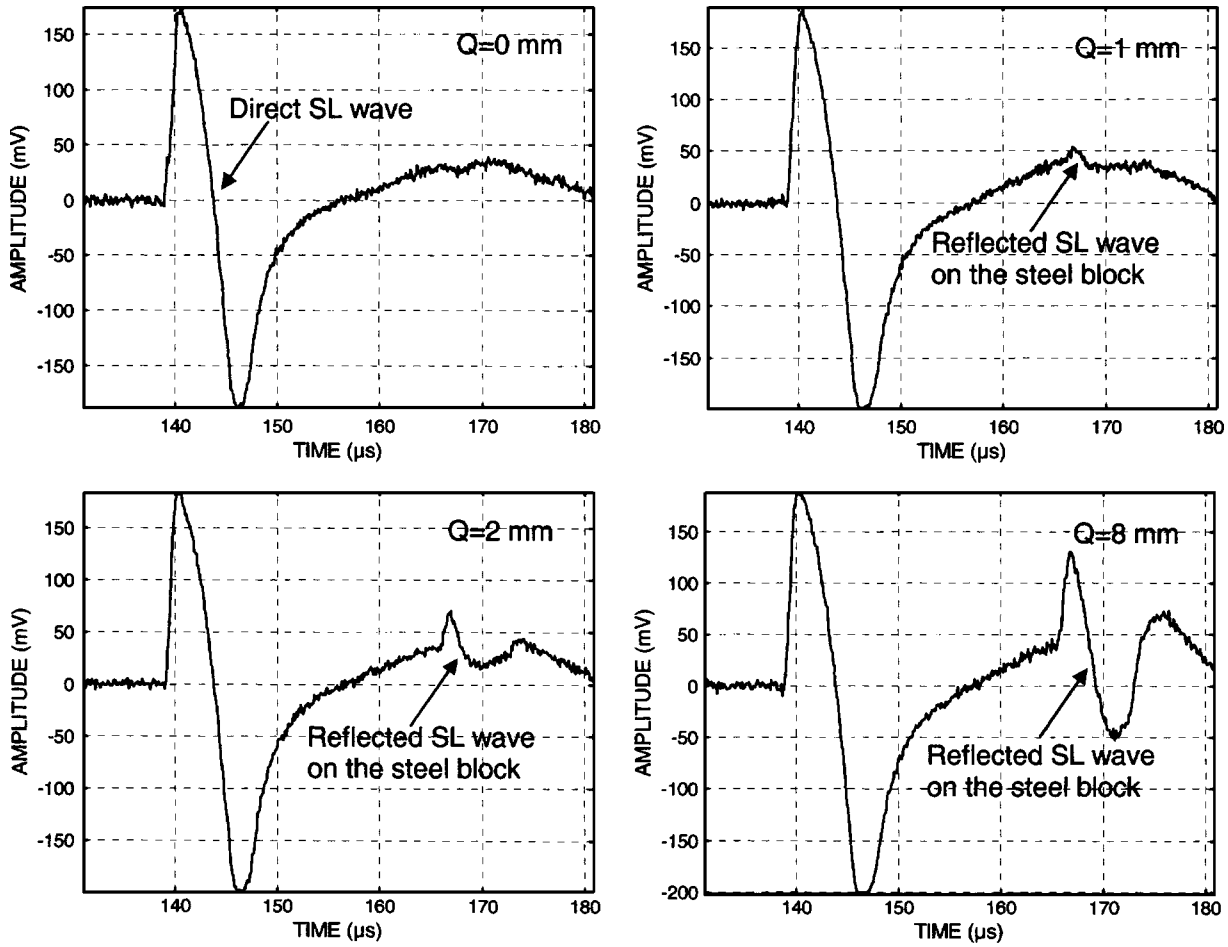

FIG. 10. Reflected SL wave on a steel block coming out from the surface of the sample of a distance Q.

surement of the SL wave comes from the air index variation. For this purpose, in contrast to the previous experiment, the interferometer beam is adjusted parallel and very close to the surface of the sample (about 0.5 mm), as described in Fig. 4. It passes through the acoustic field and is reflected by a fixed mirror. The SL wave is always very well detected, as shown in Fig. 5. Its velocity is 345.8 m/s, which is in good agreement with the previous results. This assumption is also confirmed by another experiment, which has been performed by intercepting the acoustic field in the air. The configuration is the one depicted in Fig. 1. Additionally, a perspex plate comes progressively near the surface of the sample (distance H) between the line source and the probe beam (in the $-z$ direction). At the same time, we observe a reduction of the SL wave amplitude and almost all of it is attenuated when the plate is very close to the sample, as shown in Fig. 6. Using the expressions of the displacements for the Scholte wave given in the Appendix, the theory allows us to calculate

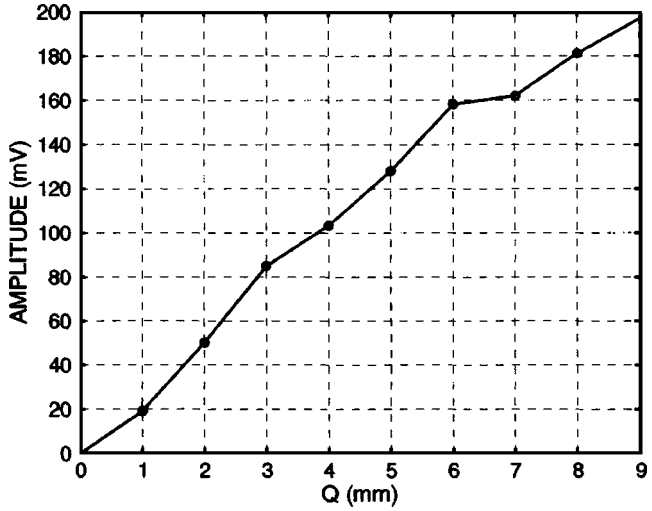

FIG. 11. Peak-to-peak amplitude of the reflected SL wave on a steel block coming out from the sample of a distance Q.

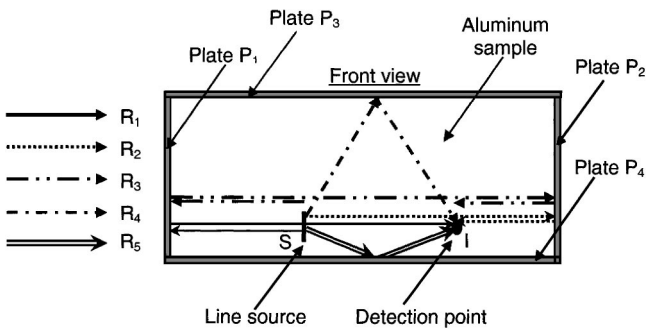

FIG. 12. Configuration used in the experiment illustrating the SL wave sizing of structures. R_1 to R_5 correspond to some possible reflections of the wave on glass plates.

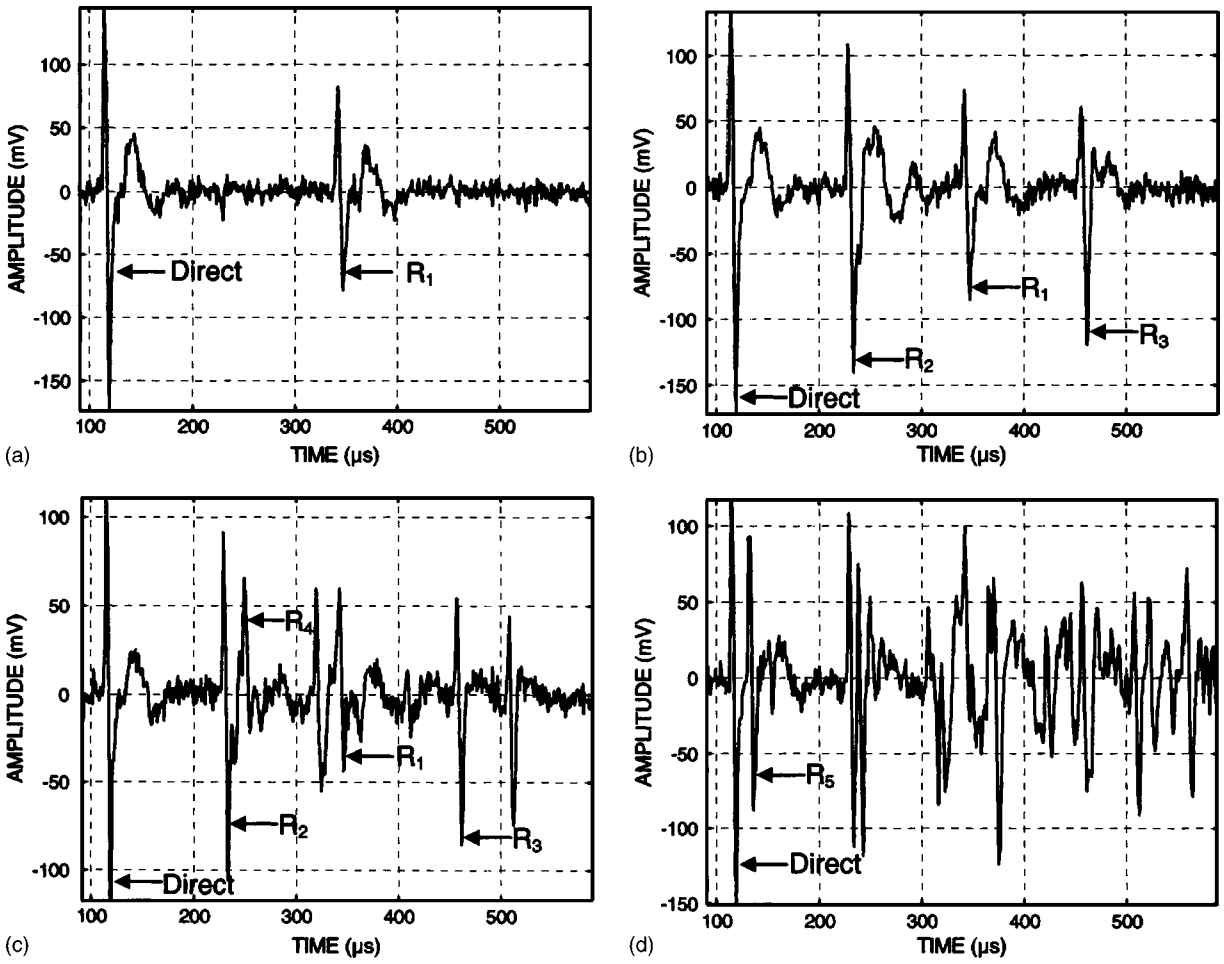

FIG. 13. Time traces of the SL wave reflections (R_1 to R_5) on glass plates stuck on the side of the aluminum sample [(a) plate P_1 only, (b) plates P_1 and P_2, (c) plates P_1, P_2, and P_3, and (d) four plates].

the ratio R' of the signal amplitude for two distances H_2 and H_1. This one is simply given by the ratio of the optical phase shifts v_i

$$R' = \int_0^{H_2} e^{-\xi_{l2} kz} dz / \int_0^{H_1} e^{-\xi_{l2} kz} dz, \tag{7}$$

where $\xi_{l2} = \sqrt{1-(V_s/V_f)^2}$. In our case, the terms $\xi_{l2} k H_{1,2} \ll 1$ and consequently, $R' \approx H_2/H_1$. This result is in good agreement with the determination of R', considering the experiments presented in Fig. 6(b) and 6(c).

IV. POTENTIAL APPLICATIONS

The previous section of this paper has described the laser generation and detection of the SL wave at the air-aluminum interface. It is now interesting to consider the interaction of this wave with different structures to know its potentialities in non-destructive testing.

A type of experiment consists of putting down some glass plates on the propagation path of the wave. A schematic representation of this experiment is provided in Fig. 7. The experimental results in Fig. 8(a) show that for each additional plate, the amplitude of the transmitted SL wave is reduced and a delay proportional to the plate thickness is

TABLE I. Comparison between the propagation distances calculated using the times of flight of the SL wave and those determined by the sizes of the structure.

SL wave reflection	SL wave time of flight (μs)	Propagation distance calculated using the SL wave time of flight (mm)	Propagation distance calculated using the sizes of the structure (mm)
R_1	344.4	118.3	118.0
R_2	231.2	79.4	80.0
R_3	458.5	157.5	158.0
R_4	252.2	86.6	86.8
R_5	134.3	46.1	46.1

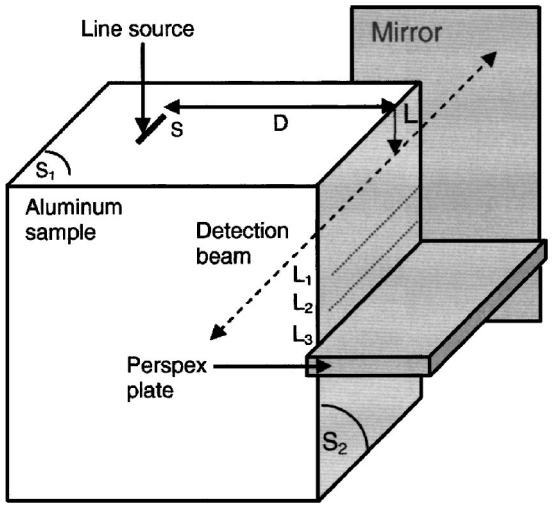

FIG. 14. Experimental setup for the detection of the diffracted SL wave under the surface of generation (S_1). D is the distance between the line source and the extremity of the solid and L corresponds to the distance along S_2. A perspex plate is used to reflect the diffracted wave at three distances (L_1,L_2, and L_3).

observed. It also appears clearly in Fig. 8(b) that the glass plates thickness is a linear function of the wave time of flight (determined by zero crossing).

In the second series of experiments, the reflection of the SL wave is investigated. A steel block comes out from the surface of the sample of a distance Q, as described in Fig. 9. We observed clearly in Fig. 10 the direct SL wave (propagation path *S-I*) and its reflection on the steel block for different distances Q. According to the time of flight of the reflected wave, the propagation path (line source-steel block-detection point) can be well determined. It corresponds to the path given by the acoustic rays theory and is depicted in Fig. 9 as (*S-C-I*). On the other hand, Fig. 11 shows that the amplitude of the reflected signal is very well linked to the parameter Q. It is clear from these results that information

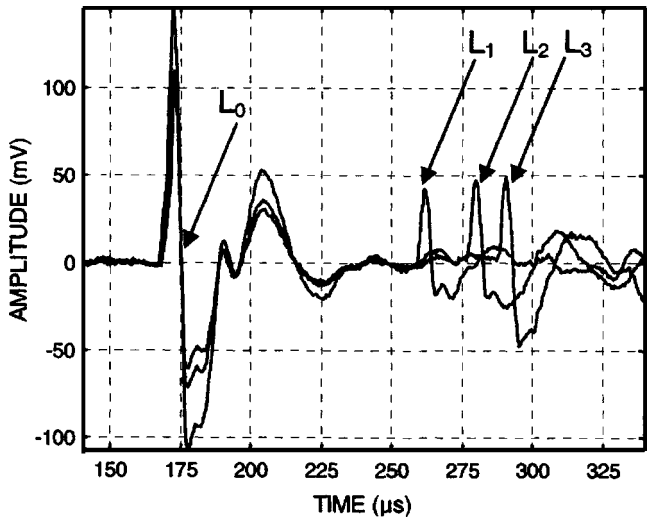

FIG. 15. SL waves detected at a distance $L_0 \approx 8.5$ mm under the surface of the acoustic excitation. Each signal clearly shows the diffracted SL wave at the extremity of the solid and its reflection on the perspex plate which is moved successively from distance L_1 to L_3 ($L_1 \approx 24$ mm, $L_2 \approx 27$ mm, and $L_3 \approx 29$ mm).

about the position of a part of an assembly can be obtained by using the SL wave. Consequently, the size of structures can also be determined. An example is given by sticking glass plates (P_1 to P_4) on each side of an aluminum block, as it is illustrated in Fig. 12. The different reflections of the SL wave on these plates are designated by R_1 to R_5 and are schematically represented in this figure. The signals observed for each additional plate are given in Fig. 13 and the different times of flight are listed in Table I. According to the SL wave velocity which is 343.6 m/s, the propagation distance can be calculated for each reflection of the wave. On the other hand, these distances can be obtained by measuring directly the dimensions of the assembly. Table I shows a good agreement between these two methods and confirms our purpose about the sizing of structures.

The aim of the last type of experiment is to show that information about the position of the inaccessible part of a sample can also be obtained by using the SL wave. In order to do this, we considered the experiment presented in Fig. 14. The wave is generated on one side of the sample (S_1) and the detection beam is located parallel to another side (S_2) at a distance $L_0 \approx 8.5$ mm from the surface S_1. Additionally, a perspex plate is moved along the surface S_2 and three positions of this plate (from S_1) are considered: $L_1 \approx 24$ mm, $L_2 \approx 27$ mm, and $L_3 \approx 29$ mm. The propagation distance D between the line source and the extremity of the solid is approximately 51.5 mm. Figure 15 presents the signals recorded for the three distances considered. In this figure, we clearly observe the diffraction[14] of the incident SL wave at the extremity of the solid and its reflection on the perspex plate. A time of flight analysis easily gives the distance between the different positions of the plate.

V. CONCLUSIONS

In this paper, we have confirmed the high efficiency of laser ultrasonics to generate the mixed Scholte-lateral wave at the air-aluminum interface. Its optical detection by heterodyne interferometer working perpendicularly to the surface of the sample leads to a high amplitude for this wave due to the predominant effect in the detection of the air index variation and not of the normal surface displacement. The detection also works without reflecting the probe beam on the sample. Consequently, the method can be used for materials with low-reflectivity surface.

Moreover, different experiments have clearly demonstrated the new potentialities in non-destructive testing of these interface waves. Indeed, the size and position of structures can be determined even if the considered parts are inaccessible.

This study encourages us to investigate the SL wave propagating along curved surfaces and to develop a finite element model for the theoretical prediction of these propagation phenomena.

APPENDIX: ENERGY FLOW OF THE SCHOLTE WAVE IN BOTH MEDIA

For the Scholte wave propagating along the x axis, the displacements are given by[15]

$$\left.\begin{aligned} u_{x,1} &= i(\xi_{t1}e^{\xi_{t1}kz} + \eta_1 e^{\xi_{l1}kz})A_0 e^{i(kx-\omega t)} \\ u_{z,1} &= (e^{\xi_{t1}kz} + \eta_1 \xi_{l1} e^{\xi_{l1}kz})A_0 e^{i(kx-\omega t)} \end{aligned}\right\}$$

$$z < 0 \text{ (in the solid, index 1)},$$

$$\left.\begin{aligned} u_{x,2} &= i\,\eta_2 e^{-\xi_{l2}kz} A_0 e^{i(kx-\omega t)} \\ u_{z,2} &= -\,\eta_2 \xi_{l2} e^{-\xi_{l2}kz} A_0 e^{i(kx-\omega t)} \end{aligned}\right\}$$

$$z > 0 \text{ (in the fluid, index 2)},$$

where $\xi_{li} = \sqrt{1-(V_s/V_{li})^2}$; $\xi_{ti} = \sqrt{1-(V_s/V_{ti})^2}$; $\eta_1 = -\left((1+\xi_{t1}^2)/2\xi_{l1}\right)$; and $\eta_2 = -\left((1-\xi_{t1}^2)/2\xi_{l2}\right)$. V_{ti} and V_{li} stand for the velocities of the shear and longitudinal waves, respectively, in the medium of index i. V_s is the velocity of the Scholte wave and k is its wave number. A_0 is an arbitrary amplitude.

The energy flows P_1 in the solid and in the fluid (P_2) are then given by the expressions

$$P_1 = \frac{-\omega|A_0|^2}{2}\left\{\frac{-\mu_1(1+3\xi_{t1}^2)}{2\xi_{t1}} + \frac{\eta_1[\lambda_1\xi_{t1}\xi_{l1}^2 - (\lambda_1+4\mu_1)\xi_{t1} - \mu_1\xi_{l1}(3+\xi_{t1}^2)]}{\xi_{t1}+\xi_{l1}} + \frac{\eta_1^2[(\lambda_1-2\mu_1)\xi_{l1}^2 - (\lambda_1+2\mu_1)]}{2\xi_{l1}}\right\},$$

$$P_2 = \frac{\omega\eta_2^2}{4}\frac{\lambda_2}{\xi_{l2}}(1-\xi_{l2}^2)|A_0|^2,$$

where λ_i and μ_i are the Lame constants of the medium i.

[1] I. A. Viktorov, Sov. Phys. Acoust. **25**, 1 (1979).
[2] L. M. Brekhovskikh, *Waves in Layered Media* (Academic, New York, 1960).
[3] B. Poirée and F. Luppé, J. Acoust. **4**, 575 (1991).
[4] M. de Billy and G. Quentin, J. Appl. Phys. **54**, 4314 (1983).
[5] C. Desmet, V. Gusev, W. Lauriks, C. Glorieux, and J. Thoen, Appl. Phys. Lett. **68**, 2939 (1996).
[6] V. V. Sychev, A. A. Vasserman, A. D. Kozlov, G. A. Spiridonorv, and V. A. Tsymarny, *Thermodynamic Properties of Air* (Hemisphere Publishing, New York, 1987).
[7] V. E. Gusev, W. Lauriks, and J. Thoen, IEEE Trans. Ultrason. Ferroelectr. Freq. Control **45**, 170 (1998).
[8] V. Gusev, C. Desmet, W. Lauriks, C. Glorieux, and J. Thoen, J. Acoust. Soc. Am. **100**, 1514 (1996).
[9] Al. A. Kolomenskii and A. A. Maznev, Sov. Phys. Acoust. **36**, 258 (1990).
[10] J. D. Aussel and J. P. Monchalin, Ultrasonics **27**, 165 (1989).
[11] C. Desmet, V. Gusev, W. Lauriks, C. Glorieux, and J. Thoen, Opt. Lett. **22**, 69 (1997).
[12] C. Chenu, M. H. Noroy, and D. Royer, Appl. Phys. Lett. **65**, 1091 (1994).
[13] C. Mattei and L. Adler, Ultrasonics **38**, 570 (2000).
[14] A. Tinel and J. Duclos, J. Acoust. Soc. Am. **95**, 13 (1994).
[15] G. D. Meegan, M. F. Hamilton, Yu. A. Il'inskiium, and E. A. Zabolotskaya, J. Acoust. Soc. Am. **106**, 1712 (1999).